The response of seismicity to Coulomb stress triggers and shadows of the 1999 M_w=7.6 Chi-Chi, Taiwan, earthquake

Kuo-Fong Ma, Chung-Han Chan

Institute of Geophysics, National Central University, Jung-Li 320-54, Taiwan, ROC.

fong@earth.ncu.edu.tw tel 886-3-4227151 x 65634 fax 886-3-4222044

Ross S. Stein

U.S. Geological Survey, Menlo Park, CA 94025

rstein@usgs.gov tel 1 650 329 4840 fax 1 650 329 5143

Abstract The correlation between static Coulomb stress increases and aftershocks has provided the strongest evidence in the literature that stress changes promote seismicity, a correlation that the Chi-Chi earthquake well exhibits. Several studies have deepened the argument by resolving stress changes on aftershock focal mechanisms, which removes the assumption that the aftershocks are optimally oriented for failure. Here one compares the percentage of planes on which failure is promoted after the main shock relative to the percentage beforehand. For Chi-Chi we find a 28% increase for thrust faults and an 18% increase for strike-slip faults, commensurate with increases reported for other large mainshocks. But perhaps the chief criticism of static stress triggering is the difficulty in observing predicted seismicity rate decreases in the stress shadows, or sites of Coulomb stress decrease. Detection of sustained drops in seismicity rate demands a long catalog with a low magnitude of completeness and a high seismicity rate, conditions that are met

at Chi-Chi. We find four lobes with seismicity rate declines of 40-90% for 50 months, and they coincide with the stress shadows for strike-slip faults, the dominant faulting mechanism. The rate drops are evident in uniform cell calculations, 100-month time series, and by visual inspection of the M≥3 seismicity. Another reason why detection of such declines has proven so rare emerges from this study: there is a ubiquitous increase in seismicity rate for the first 3 months after Chi-Chi—and perhaps several other mainshocks—that must be associated with a different mechanism.

1.0 Introduction

Advocates of static stress transfer argue that aftershocks and subsequent mainshocks often occur in regions that experienced an increase in Coulomb stress caused by the mainshock, and are less prevalent in regions subject to a Coulomb stress drop (see reviews by Harris, 1998; Stein, 1999; King and Cocco, 2001). But to date, most work has concentrated on earthquakes on strike-slip faults, whose stress change does not vary greatly with depth. For thrust faulting, the stress change becomes strongly depth-dependent (Lin and Stein, 2004), and thus the down-dip geometry and slip of the source fault, and the depth of aftershocks become critical to Coulomb analysis. The 20 September 1999 M_w=7.6 Chi-Chi, Taiwan, earthquake on the Chelungpu fault is probably the world's best recorded continental thrust event, with well determined spatial slip models from seismic, strong motion, and geodetic data. Its background seismicity and aftershock sequence are also recorded in unprecedented detail, making it ideal for investigation.

Several studies (e.g. Ma et al., 2001, Zeng and Chen, 2001, Chi et al., 2001; Ji et al., 2003) have illuminated the kinematics of the Chi-Chi rupture process. Results of these

studies show consistent features, with high slip in the northern portion of the fault. The aftershocks, recorded by the Central Weather Bureau Seismographic Network (CWBSN), are widely distributed over the island of Taiwan. During the first month after the mainshock, nine M>6.0 aftershocks occurred adjacent to the source region of the mainshock, yielding more disastrous damage, and providing a further dataset for stress transfer investigations.

Several Coulomb stress analyses of the 1999 Chi-Chi earthquake have already been carried out; these use the first year of aftershocks, independent of their focal mechanisms. Wang and Chen (2001) examined stress transfer to the aftershock triggering and the surrounding faults, employing a Chi-Chi source model derived from GPS data by Wang et al. (2001), which is largely inconsistent with models derived from strong motion, teleseismic and GPS data as stated previously. Wang et al. (2003) calculated the static stress transfer from 'stressgrams' derived directly from seismograms rather than from elastic calculation. The stress patterns they found are inconsistent with the expected stress change pattern associated with a thrust fault, and with the aftershock distribution (Lin and Stein, 2004), and are thus difficult to evaluate or verify.

Using the detailed spatial slip distribution of the Chi-Chi earthquake source, we calculated the Coulomb stress changes following Toda et al. (1998), which we compare to the seismicity rate changes derived from the 100-month seismic record centered on the mainshock. We focus particular emphasis on the response of seismicity to the broad lobes of calculated stress increase (the trigger lobes), and stress decrease (shadow lobes), and on whether the stress imparted to the aftershock planes promoted their failure.

2.0 Changes in Seismicity associated with the Chi-Chi earthquake

2.1 Seismicity

Our goal is to measure long-term seismicity rate changes caused by the 1999 Chi-Chi earthquake. Here, seismicity rate change is simply the rate of earthquakes after the main shock, divided by the rate beforehand. To permit visual inspection of the numerical results, we consider equal 50-month periods before and after the earthquake. We choose this duration because network detection improved substantially in 1994, when the Taiwan Telemetered Seismographic Network was upgraded and transferred to the Central Weather Bureau to become the Taiwan Seismographic Network, or CWBSN. The seismicity rate is reckoned independent of magnitude, and so it is essential that we count earthquakes above the minimum magnitude of completeness, M_c (Wiemer and Wyss, 2000).

For the post-Chi Chi period, we consider the 50-month period beginning 3 months after the mainshock. As will be evident from the time series we will shortly introduce, there is a widespread increase in seismicity throughout Taiwan during the first 1-3 months after the Chi-Chi mainshock. After this period, several areas exhibit seismicity rate declines that we will explore. The seismicity increase observed during the first few months may be caused by dynamic stresses or shaking effects, a phenomenon investigated by Gomberg et al (1998) for other earthquakes. During the first 1-3 months after the mainshock, M_c is also higher than later, presumably because the order-of-magnitude increase in seismicity overwhelms routine processing.

The distribution of M≥2.0 seismicity before and after the occurrence of the 1999 M=7.6 Chi-Chi earthquake (Figure 1) is surprisingly similar. The earthquakes are a consequence of the collision of the Philippine Sea Plate and Eurasian Plate as the Rukyu Arc, and the opening of Okinawa trough in northeastern Taiwan. The Chi-Chi earthquake itself occurred in a relatively quiet seismic region. Although the rate of seismicity within several fault lengths of the Chi-Chi epicenter is more than hundred times higher after the mainshock, the spatial distribution is only subtly changed from the pre-Chi Chi period. In fact, if one were to regard Figure 1a and Figure 1b separately, it would be difficult to tell which map contains the Chi-Chi aftershocks. We suggest that this similarity arises because stress increases amplify the rate of background seismicity, while stress decreases suppress the background seismicity. This prediction of rate/state friction (Dieterich, 1994), which regards aftershocks simply as dramatically higher rates of background seismicity, has been investigated by Toda and Stein (2003) for the 1997 Kagoshima, Japan, earthquakes, and by Toda et al (2005) for the 1992 Landers-1999 Hector Mine sequence.

2.2 Focal mechanisms

Figure 2 shows the distribution of the focal mechanisms before and after the Chi-Chi earthquake. For this new compilation, we used moment tensors inverted from waveforms of the Broadband Array in Taiwan for Seismology (BATS) (Kao et al., 2002, Liang et al., 2003, Liang et al., 2004a). Since 2001, the Data Management Center of the Institute of Earth Sciences (DMC-IES) has reported and archived moment tensor solutions obtained by inverting BATS waveforms of felt earthquakes that occurred since July 1995 (Liang et al., 2004b). The DMC-IES has reported a completed moment magnitude (M_w) of 4.2

before 2001 and 3.9 since that time. For $M_w \geq 4.0$ earthquakes with depths less than 33 km, the compilation includes 101 focal mechanisms before the Chi-Chi mainshock, and 354 afterwards. The compilation can be accessed from the website, (http://eqkc.earth.ncu.edu.tw/FocalMech).

The focal mechanisms are mainly strike-slip and thrust. There is an extended zone of seismicity in the fold and thrust belt near the ends of the Chelungpu fault dominated by strike-slip mechanisms associated with no mapped active faults. The focal mechanism distribution is generally similar before and after the Chi-Chi earthquake, except for a relative increase in strike-slip mechanisms to the southeast of the Chelungpu fault and well offshore to the east. In addition, thrust events may be relatively more common on the central east coast after the Chi-Chi earthquake.

2.3 Seismicity Rate changes

To examine the seismicity rate change, we first calculate the minimum magnitude of completeness, M_c, for the pre- and post-Chi Chi periods (Figure 3), using ZMAP (Wiemer, 2001). Where seismicity rates are low, we resort to a larger cell size to capture a sufficient number of earthquakes. M_c is generally stable throughout this 100-month period, except in the north central part of Taiwan, where M_c is higher after Chi-Chi. For the interior of Taiwan, $M_c \leq 2$; for regions within about 100 km of the coastline, $M_c \leq 3$.

The seismicity rate change is calculated in Figure 4. Within Taiwan, $M \geq 2$ is used with a 20 x 20 km cell size; for most offshore areas, $M \geq 3$ is used with a 40 x 40 km cell size. A

broad area of seismicity rate increase is seen over much of central Taiwan, with weaker and more restricted zones of seismicity rate drop in some surrounding areas.

While the seismicity rate change plot is objective, it is difficult to see the rate changes because of the high density of M≥2 shocks in Figure 1. So in Figure 5, a map of the M≥3 seismicity is also shown. Because the pre-Chi Chi shocks are red and the post-Chi Chi shocks are blue, areas dominated by red correspond to seismicity rate drops. The sites of rate increase, highlighted in light orange, dominate central Taiwan. The seismicity rate decreases are highlighted in turquoise and given a locality name. These regions are also evident in Figure 4, but their full extent is more apparent in Figure 5. Time series of seismicity in each of these regions, plotted at the highest M_c of the pre- or post-Chi Chi periods for each zone, is shown in Figure 6. For the Taichung zone off the west coast, we calculate that $M_c \geq 2.75$. All of the time series in Figure 6 exhibit a spike in seismicity during the first few months of Chi-Chi, with the top four series followed by a pronounced decline of at least 40%. It is also intriguing that for Huatung, the post-Chi Chi rate appears to recover with time.

Marsan (2003) and Felzer and Brodsky (2005) argue that seismicity rate declines are absent in the vicinity of the mainshocks they have examined. Thus we accord particular attention to the identification of seismicity rate decreases. Because such a rate decrease can result from a decaying aftershock sequence associated with a mainshock occurring during the pre-Chi Chi period, rather than with a change in rate associated with the Chi-Chi earthquake, we excluded cases influenced by such an aftershock sequence.

3.0 Coulomb Stress Changes caused by the Chi-Chi earthquake

3.1 Resolving stress changes on receiver faults

The static Coulomb stress change $\Delta CFF = \Delta\tau + \mu'\Delta\sigma$, where $\Delta\tau$ is the shear stress change (reckoned positive in the fault slip direction), μ' is effective friction coefficient (after accounting for pore fluid pressure), and $\Delta\sigma$ is the normal stress change (positive when unclamped) (King et al., 1994; Toda et al., 1998). Fault friction μ' is often inferred to be 0.4-0.8 for faults with relatively little cumulative slip, which tend to be rough; and 0.0-0.4 for faults with great cumulative slip or high pore pressure, which tend to be smooth or well-lubricated (Parsons et al, 1999). Here, we use $\mu'=0.4$ because we are unable to assign a value with confidence. Major faults, such as the Chelungpu (which has slipped at 8.5 mm/year for the past 1900 years; Chen et al., 2004; Ma and Chiao, 2003) may have low friction, but for most faults the data is insufficient. We experimented with values $0.0 \leq \mu' \leq 0.8$; results are modestly sensitive to μ'.

The Coulomb stress change is a tensor quantity, and so depends not only on the source fault geometry and slip, but also on the geometry and rake of the 'receiver' or target faults that surround the source. There are two principle approaches to calculating the Coulomb stress changes on receiver faults. One can resolve the Coulomb stress changes on faults with known geometry and rake, or one can resolve stress changes on 'optimal planes' constrained by the tectonic or regional stress.

We resolve the Coulomb stress change on planes optimally oriented for failure with

respect to the regional stress plus earthquake stress change (King et al, 1994). The faults on which earthquakes at the magnitude of completeness, M_c, of 2.0-3.0, can occur are quite small, with rupture lengths as little as 50 m. At this scale, there are likely myriad faults with different geometries and rakes at any given position in the crust. So, we consider optimum planes. The regional stress is typically inferred from focal mechanisms far from the source fault, borehole stress inversions, or the geodetically determined strain rate tensor. At every calculation point, the earthquake stress is added to the regional stress to get a new, local stress tensor.

The relationship between the principal compression axis and the optimal planes is shown in Figure 7a-b atop each map. The optimal planes are oriented with respect to the local stress tensor. The optimal strike-slip planes dip vertically; the optimal thrust plans dip at shallow angle and strike perpendicular to the axis of principal compression. The internal angle between the optimal planes is a function of friction, μ‘. For μ‘=0, at each point the two optimal planes are mutually orthogonal; for a high value of friction, they form at acute angles to each other. For central Taiwan, a regional compressive stress of 100 bars acting in the direction of the stress axis of the Philippine Sea to the Eurasian Plates (Seno, 1977) is used, with a 30 bar compression oriented vertically; the full stress tensor is listed in Table 1.

3.2 Coulomb stress change for an idealized Chi-Chi source

Stress transfer associated with the Chi-Chi earthquake is perhaps best understood by considering Figure 7, in which the maximum Coulomb stress change over a depth of

5-30 km is calculated for a simplified Chi-Chi source with M_w=7.6. Here, we make an additional assumption that at every point on the earth's surface, aftershocks, or seismicity rate increases, will occur at the depth where the Coulomb stress change is most positive. Unlike the Coulomb stress calculated at a particular depth horizon, the maximum Coulomb stress change, when integrated around a source, will have a net positive value; the trigger zones will enlarge and the stress shadows will shrink. This approach is most amenable to examinations of seismicity rate changes or aftershocks over the entire brittle crust, or the uppermost 25-30 km. In Figure 7a-b, the source is pure thrust slip; the observed left-lateral component is ignored. Figure 7a shows the stress changes on surrounding thrust faults; Figure 7b shows the stress changes on strike-slip faults. Stress changes on strike-slip receiver faults extend farther from the source than for thrust faults, the trigger zones forming a characteristic 'butterfly' pattern (Stein et al, 1994), and the shadows are quite deep.

A calculation that more closely resembles the Chi-Chi earthquake is shown in Figure 7c-d, for a source with a strike of 3° and a rake of 66° (the CMT rake for the Chi-Chi main shock), and with the regional compression axis is oriented NW-SE, as in central Taiwan. For thrust faults, there is a broad zone of stress increase across central Taiwan; for strike-slip faults, the butterfly wings become asymmetric, but the four stress shadows—large shadows extending offshore and small ones to the north and south of Taiwan—persist.

Although we will next introduce a detailed model of the Chi-Chi source, it is instructive that even this simple model captures much of the observed pattern of seismicity rate

change evident in Figure 4 and Figure 5. In addition, the observed pattern of seismicity rate changes is more similar to the expectation for strike-slip than thrust faults, and so we superimpose the stress contours of Figure 7d on Figure 4. Although numerous thrust faults are evident in central Taiwan, the majority of the aftershock focal mechanisms, particularly in central Taiwan, are strike-slip (Figure 2).

3.3 Coulomb stress change for a detailed Chi-Chi source

For a rigorous comparison between stress change and seismicity change, we use the full variable-slip source of Ji et al. (2003), which was inverted from GPS displacements, strong motion data, and teleseismic waveforms. The coseismic source is defined by 324 slip patches with variable rake and slip on three rectangular planar surfaces, each dipping 29° (Figure 8). The resulting Coulomb stress changes on optimally oriented strike-slip, thrust and normal faults are shown in Figure 9. Because of the complex fault geometry and slip heterogeneity, the stress change varies with depth and along with strike. Close to the Chelungpu fault source, the stress generally increases because of the slip variability, which causes spikes in stress.

3.4 Stress change analyzed by depth and focal mechanism

The stress patterns for thrust (Figure 9a) and strike-slip (Figure 9b) receiver faults are similar to that shown in Figure 7c-d for an idealized Chi-Chi source, and the pattern for normal receiver faults is roughly opposite as that for thrust faults. In comparison to the maximum Coulomb stress change independent of depth (Figure 7), in Figure 9 the

stress shadows are larger. This is because, in each depth slice, the extent of the triggering zones and shadows will be approximately equal, and so ~50% of a random earthquake sample would lie in regions of positive Coulomb stress change.

To examine the correlation of the Coulomb stress changes to earthquakes with focal mechanisms, in Figure 9 earthquakes before (green) and after Chi-Chi (magenta) are also plotted in the depth slices by rake angle (thrust, 45° to 135°; strike-slip, -45° to 45°; normal, -45° to -135°). Only the post-Chi Chi mechanisms should exhibit a correlation with the Coulomb stress change. Some 75% of the post-Chi Chi focal mechanisms in Figure 9 occur in zones of Coulomb stress increase; this percentage is the same for all three mechanisms. This ratio is constant despite the much higher percentage of strike-slip mechanisms, which comprise 64% of the focal mechanism catalog.

3.5 Stress resolved on all M≥4 earthquakes with focal mechanisms

While Figure 9 affords visual inspection of the relationship between the calculated stress and the focal mechanisms, and shows the depth distribution of stress and earthquakes, we can more fully exploit the focal mechanisms by calculating the Coulomb stress changes on the nodal planes of each of the 354 events. Unlike Figure 9, which simply classifies events into one of three mechanisms and four depth ranges, here we resolve the stress change at the observed depth and for the observed strike, dip, and rake. For zero friction (μ'), the Coulomb stress change on both nodal planes is the same, but for non-zero friction it is different, introducing a nodal plane ambiguity. In Figure 10a, we bin the mechanisms by the resolved Coulomb stress change as a function of focal

mechanism, under the zero-friction assumption. For 74% of the thrust, 61% of the strike-slip, and 63% of the normal events, the calculated stress change exceeds 0.01 bars, whereas for random occurrence, failure would be promoted on about 50% of the events. For stress changes > |0.1 bars|, the comparison is stronger still: 85% of the thrust, 65% of the strike-slip, and 80% of the normal events are brought close to Coulomb failure. These percentages rise slightly for strike-slip and thrust mechanisms if we omit the first three months of focal mechanisms.

To include the role of unclamping in promoting failure, which several studies suggest is important (Hardebeck et al, 1998; Parsons et al, 1999; Seeber and Armbruster, 2000; Lin and Stein, 2004), (letting $\mu'=0.4$), we must contend with the nodal plane ambiguity. We do so by comparing post-Chi Chi to pre-Chi Chi mechanisms shown in Figure 2a. If both nodal planes are brought closer to failure, we report the smaller stress change of the two; if failure is promoted on only one plane, we report its value. If both planes receive a Coulomb stress drop, we report the smaller decrease. This selection criterion is applied to both pre- and post-Chi Chi events in Figure 10b-c, an approach introduced by Hardebeck et al (1988). As shown in Figure 10d, the percentage of thrust events with Coulomb stress changes > |0.1 bars| rose by 26% after Chi-Chi (from 37 to 63%); for strike-slip events, it rose by 18% (from 32 to 50%). The pre-Chi Chi sample of 5 normal events is too small to be reliable.

3.6 Stress imparted to M≥6 aftershocks

Thus far, we have focused on the 92,000 M≥2 earthquakes, and the smaller but

richer sample of M≥4 focal mechanisms. For earthquake hazards, however, we are most concerned about M≥6 shocks, of which 10 have struck within 50 km of the mainshock (Figure 2b, inset). The quality of the Taiwan network makes it possible to attempt to distinguish the likely fault plane from the auxiliary plane, which is needed for the stress analysis for μ'=0.4. Yen (2002) used strong motion waveforms to determine the likely rupture planes and spatial slip distributions, and relocated the aftershocks using HypoDD (Waldhauser and Ellsworth, 2000). Chi and Dreger (2004) inverted strong motion data for the finite fault source parameters, and derived a preferred plane from forward testing of focal mechanisms, hypocenters and rupture velocities (Table 2). Most of the likely fault planes dip to the east (Figure 2b inset and Table 2), consistent with the fold and thrust tectonics.

For the 10 shocks, there are 16 preferred rupture planes based on analyses by Ma and Wu (2001), Yen (2002), and Chi and Dreger (2004). Failure on 12-14 of the preferred rupture planes, or 7-9 of the earthquakes, is calculated to have been promoted by the Chi-Chi mainshock alone, and by the cumulative stress change from Chi-Chi and the successive M≥6 shocks; the median stress change on the 16 planes is +4.4 bars (Table 2).

4.0 Discussion and Conclusions

This study benefited from an extraordinary catalog of M≥2 earthquakes with nearly uniform dense station coverage for 50 months before and 50 months after the Chi-Chi earthquake (Figures 1 and 3), without which would be nearly impossible to identify and

measure seismicity rate drops associated with large earthquakes. We also were able to subject 455 M≥4 relocated earthquakes with focal mechanisms to stress analysis, aided by a 325-patch earthquake source model. Finally, we could examine the stress imparted to 10 M≥6 aftershocks for which the likely rupture planes have been distinguished (Figure 2b inset). From this work we draw several principal conclusions:

4.1 Aftershocks and the permanence of background seismicity patterns

The pre-Chi Chi and post-Chi Chi patterns of seismicity patterns are surprisingly similar, particularly given that the post-seismic period contains 13,382 more shocks than the preceding period of the same duration (Fig. 1). This, in our judgment, is an indication that seismicity is not turned on or off by a mainshock, but rather, the rate of earthquakes rises in areas of Coulomb stress increase, and falls in regions of stress decrease, as predicted by rate/state friction (Dieterich, 1994; Toda et al, 2005). Areas of very low background seismicity do not light up in aftershocks regardless of the Coulomb stress increase or their proximity to the mainshock rupture surface, whereas sites of high background seismicity are very sensitive to small stress increases or decreases.

4.2 Seismicity rate decreases in the stress shadows

We observe a widespread seismicity rate jump within 150 km of the Chi-Chi epicenter during the first several months of the main shock, regardless of the calculated Coulomb stress change. Following this initial period, there are four principal regions of seismicity rate decline. We have excluded apparent drops caused by decaying aftershocks of

mainshocks that occurred during the pre-Chi Chi period. The remaining seismicity rate drops are evident in uniform cell sampling (Figure 4), and can be visually confirmed by M≥3 seismicity (Figure 5). In these regions the seismicity rate decreases by 40-90% (Figure 6). The Nansan and Kaoping zones fall into the Coulomb stress shadows for strike-slip faults, but not for thrust faults. Focal mechanisms of pre- and post-Chi Chi earthquakes in these zones are dominated by strike-slip events (Figure 9b). For Huatung, which has the highest background seismicity rate, the seismicity rate may recover to pre-Chi Chi levels by the end of the 50-month period. Such behavior would be consistent with rate/state friction if the stressing rate were higher here than elsewhere.

The sites of seismicity rate changes resemble the calculated Coulomb stress change, whether we use a simple, idealized source (Figure 7b-c) or the detailed source (Figure 9a-c), from which we conclude that the stress shadows do, indeed, cause the rate of earthquakes to drop. The existence of four zones of post-Chi Chi seismicity rate drop, and their association with Coulomb stress shadows, is a critical element of the Coulomb hypothesis, because it is an attribute unique to the static stress change. Observations of seismicity rate drops are only possible when background seismicity rates are high and seismic station is dense. Felzer and Brodsky (2005) argue that seismicity rate declines associated with mainshocks do not occur, and take issue with reported rate declines associated with the 1989 M=6.9 Loma Prieta (Parsons, 2002), 1983 M=6.7 Coalinga (Toda and Stein, 2002), and 1992 Landers (Wyss and Wiemer, 2000) shocks. In our judgment, the Chi-Chi result, together with similar findings for the 1997 M=6.5 Kagoshima (Toda and Stein, 2003; Woessner et al, 2004) and 1999 M=7.1 Hector Mine (Toda et al, 2005) shocks, strengthens the case for the role of stress shadows in

suppressing seismicity.

4.3 Focal mechanisms confirm the role of Coulomb stress changes

When we shed the optimal orientation assumption and resolve stress changes on the nodal planes of the post-Chi Chi shocks: 85% of the thrust and 65% of the strike-slip events receive calculated shear stress increases greater than 0.1 bar. To examine the Coulomb stress, which includes the role of unclamping in promoting failure, we can only measure the percentage increase after the Chi-Chi earthquake with confidence. Here we find a 26% increase in thrust events, and a 18% increase in strike-slip events receiving a Coulomb stress change greater than 0.1 bar. By comparison, Hardebeck et al (1998) and Hardebeck and Hauksson (1999) reported a 25% increase for Landers and a 20% increase for Northridge, and Seeber and Armbruster (2000) found a 30% increase for Landers (all three are plotted in Stein, 1999). Finally, no other mainshock examined by Coulomb analysis has Chi Chi's abundance of large aftershocks; 7-9 out of 10 M≥6 shocks receive a positive Coulomb stress change, with a mean stress increase of 4.4 bars.

4.4 Is the signature of dynamic stress triggering in the first postseismic months?

We speculate that the ubiquitous seismicity rate increase lasting for 1-3 months (Figure 6) is probably a general phenomenon caused by dynamic stress triggering. Parsons (2002) observed a similar phenomenon following M≥7 shocks in the Harvard CMT catalog, in which regions within 100 km of the mainshock subjected to a calculated shear stress drop showed a five-fold increase in seismicity rate during the first binned interval, in this case,

1 yr. A similar but somewhat muted rate increase on planes calculated to be subjected to a Coulomb stress decrease for 2-4 months following the 1992 Landers earthquake is apparent in time the series of Seeber and Armbruster (2000). Similarly, where the shear stress shadow of the 1983 Coalinga earthquake is traversed by the San Andreas fault, the seismicity rate does not drop for 4 months (Toda and Stein, 2002). But in contrast, the rate decrease associated with the second of the 1997 Kagoshima couplet is immediate (Toda and Stein, 2003). We suggest that a fruitful avenue of research would be to isolate and identify the pattern of this transient seismicity rate increase, to see where it might lead us in the quest to understand earthquake triggering.

Acknowledgements. We are grateful for reviews by William Bakun and Delphine Fitzenz, Joan Gomberg, and two anonymous referees. We thank Dr. W.-Z. Liang and the Central Weather Bureau Seismological Center for providing the complete seismic catalog and the BATS CMT solutions from DMC-IES.

References

Chi, W.-C., D. Dreger, and A. Kaverina, Finite-source modeling of the 1999 Taiwan (Chi-Chi) earthquake derived from a dense strong-motion network, *Bull. Seismol. Soc. Am.*, 91, 1144-1157, 2001.

Chi, W.-C., and D. Dreger, Crustal deformation in Taiwan: Results from finite source inversions of six Mw > 5.8 Chi-Chi aftershocks, J. Geophys. Res., 109, B07305, doi:10.1029/2003JB002606, 2004.

Chen, W.-S., K.-J. Lee, L.-S. Lee, D. J. Ponti, C. Prentice, Y.-G. Chen, H.-C. Chang, and Y.-H. Lee, Paleoseismology of the Chelungpu fault during the past 1900 years., Quaternary International, *115-116, 167-176, 2004.*

Dieterich, J., A constitutive law for rate of earthquake production and its application to earthquake clustering, *J. Geophys. Res.*, *99* (B2), 2601-2618, 1994.

Felzer, K.R., and E. Brodsky, Testing the stress shadow hypothesis, submitted to *J. Geophys. Res.*, 2005.

Hardebeck, J. L., J. J. Nazareth, and E. Hauksson, The static stress change triggering model: Constraints from two southern California aftershocks sequences, *J. Geophys. Res.*, 103, 24,427– 24,437, 1998.

Hardebeck, J. L. and E. Hauksson, Background stress state plays a role in earthquake triggering. Eos Trans. AGU 80 (46), Fall Meet. Suppl., pp. 1005, 1999.

Harris, R. A., Introduction to special section: Stress triggers, stress shadows, and implication for seismic hazard, *J. Geophys. Res.*, 103, 24347-24358, 1998.

Gomberg, J., N.M. Beeler, M.L. Blanpied, and P. Bodin, Earthquake triggering by transient and static deformations, *J. Geophys. Res.*, *103*, 24,411-24,426, 1998.

Ji, C., D. V. Helmerger, D. J. Wald, K.-F. Ma , Slip history and dynamic implications of the 1999 Chi-Chi, Taiwan, earthquake. *J. Geophys. Res.* 108, B9, 2412, doi:10.1029/2002JB001764, 2003.

Kao, H., Y.-H. Liu., W.-T. Liang, and W.-P. Chen, Source parameters of regional earthquakes in Taiwan: 1999-2000 including the Chi-Chi earthquake sequence, TAO, 13, 279-298., 2002.

King, G. C. P., R. S. Stein, and J. Lin, Static stress changes and the triggering of earthquakes, *Bull. Seis. Soc. Amer.*, 84, 935-953,1994.

King, G. C. P., and M. Cocco, Fault interaction by elastic stress changes: New clues from earthquake sequences, Adv. Geophys, 44, 1-28, 2001.

Liang, W.-T., Y.-H. Liu, H. Kao, Source parameters of regional earthquakes in Taiwan: Januanry-December 2001, TAO, 14, 249-260, 2003.

Liang, W.-T., Y.-H. Liu, H. Kao, Source parameters of regional earthquakes in Taiwan: January-December 2002, TAO, 15, 727-741, 2004a.

Liang, W.T., Y.H. Liu, H. Kao and B.S. Huang, Introduction to the centroid moment tensor catalog database of Taiwan: a key issue of the broadband array in Taiwan for seismology (BATS), Abstract, European Seismological Commission XXIX General Assembly, SCB-1, 66, 2004b.

Lin, J. and R.S. Stein, Stress triggering in thrust and subduction earthquakes, and stress interaction between the southern San Andreas and nearby thrust and strike-slip faults, *J. Geophys. Res.*, 109, B02303, doi:10.1029/2003JB002607, 2004.

Ma, K.-F., J. Mori, S.-J. Lee, and S.-B. Yu, Spatial and temporal distribution of slip for the 1999 Chi-Chi, Taiwan earthquake, *Bull. Seis. Soc. Am.*, 91, 1-19, 2001.

Ma, K.- F. and S.- I. Wu, Quick slip distribution determination of moderate to large inland

earthquakes using near-source strong motion waveforms, *Earthquake Engineering and Earthquake Seismology*, 3, 1-10, 2001.

Ma, K.-F., and L.-Y. Chiao, Rupture behavior of the 1999 Chi-Chi, Taiwan, earthquake-slips on a curved fault in response to the regional plate convergence, *Engineering Geology*, 71, 1-11, 2003.

Marsan, D., Triggering of seismicity at short timescales following California earthquakes, *J. Geophys. Res.*, *108*, doi:10.1029/2002JB001946, 2003.

Parsons, T., R. S. Stein, R. W. Simpson and P. A. Reasenberg, Stress sensitivity of fault seismicity: A comparison between limited-offset oblique and major strike-slip faults, J. Geophys. Res., 104,. 20,183-20,202, 1999. Parsons, T., Global observation of Omori-law decay in the rate of triggered earthquakes: Large aftershocks outside the classical aftershock zone, J. Geophys. Res., 107, 2199, doi:10.1029/2001JB0006462, 2002.

Seeber, L., and J. G. Armbruster, Earthquakes as beacons of stress change, *Nature*, 407, 69-72, 2000.

Seno, T. The instantaneous rotation vector of the Philippine Sea Plate relative to the Eurasian Plate, *Tectonophysics*, 42, 209-226, 1977.

Stein, R. S., G. C. P. King, and J. Lin, Stress triggering of the 1994 M=6.7 Northridge, California, earthquake by its predecessors, *Science*, 265, 1432-1435, 1994.

Stein, R. S., The role of stress transfer in earthquake occurrence, *Nature*, 402, 605-609, 1999.

Toda, S., R. S. Stein, P. A. Reasenberg, J. H. Dieterich, and A. Yoshida, Stress transferred by the Mw=6.9 Kobe, Japan, shock: Effect on aftershocks and future earthquake probabilities, *J. Geophys. Res.*, 103, 24,543-24,565, 1998.

Toda, S., and R.S. Stein, Response of the San Andreas fault to the 1983 Coalinga-Nuñez Earthquakes: An application of interaction-based probabilities for Parkfield, J. Geophys. Res., 107, 10.1029/2001JB000172, 2002.

Toda, S., and R.S. Stein, Toggling of seismicity by the 1997 Kagoshima earthquake couplet: A demonstration of time-dependent stress transfer, J. Gophys. Res., 109, B02303, doi: 10.1029/2003JB002527, 2003.

Toda, S., R. S. Stein, K. Richards-Dinger and S. Bozkurt, Forecasting the evolution of seismicity in southern California: Animations built on earthquake stress transfer*, J. Geophys. Res., in press*, doi:10.1029/2004JB003415, 2005.

Waldhauser, F., W. L. Ellsworth , A Double-difference earthquake location Algorithm: method and application to the northern Hayward fault, California, *Bull. Seism. Soc. Am.*, 90, 1,353-1,368, 2000.

Wang, W.-H., S.-H. Chang, and C.-H. Chen, Fault slip inverted from surface displacements during the 1999 Chi-Chi, Taiwan, earthquake, Bull. Seism. Soc. Am. 91, 1167-1181, 2001.

Wang, W.-H., and C.-H. Chen, Static stress transfer by the 1999 Chi-Chi, Taiwan, earthquake: effects on the stability of teh surrounding fault systems abd aftershock triggering with a 3D fault-slip model, Bull. Seism. Soc. Am., 91, 1041-1052, 2001.

Wang, J.-C., C.-F. Shieh and T.-M. Chang, Static stress changes as a triggering mechanism of a shallow earthquake: case study of the 1999 Chi-Chi (Taiwan) earthquake, Phys. Earth. Planetary Interiors, 135, 17-25, 2003.

Wiemer, S., A software package to analyse seismicity: ZMAP, *Seismol. Res. Letts.*, *72* (3), 373-382, 2001.

Wiemer, S., and M. Wyss, Minimum magnitude of completeness in earthquake catalogs:

Examples form Alaska, the western United States, and Japan, *Bull. Seismol. Soc. Amer.*, *90*, 859-869, 2000.

Woessner, J., E. Hauksson, S. Wiemer, and S. Neukomm, S.The 1997 Kagoshima (Japan) earthquake doublet: A quantitative analysis of aftershock rate changes, Geophys. Res. Let., 31, L03605, doi:10.1029/2003GL018858, 2004.

Wyss, M. and S. Wiemer, Change in probability for earthquakes Landers in southern California due to the magnitude 7.3 earthquake. *Science 290*, 1334–1338, 2000.

Yen, Y.-T., Slip distribution of Mw 6.0 aftershocks of the 1999 Chi-Chi Taiwan Earthquake., M.Sc. Dissertation, National Central University, Jung-Li, pp.122, 2002.

Zeng, Y. H., and C. H. Chen, Fault rupture process of the 20 September 1999 Chi-Chi, Taiwan, earthquake., Bull. Seism. Soc. Am. 91, 1088-1098, 2001.

Table Captions

Table 1. Regional or tectonic stress tensor used to calculate the Coulomb stress change on optimally oriented faults in Figure 7b-c and Figure 9. The principal compression axis for this stress tensor, along with optimal orientations of thrust and strike-slip faults far from the Chi-Chi source, are shown in Figure 7b-c.

Table 2. Coulomb stress changes (for μ'=0.4) imparted by the Chi-Chi mainshock, and by Chi-Chi plus successive M≥6 shocks, resolved onto the preferred plane of each M≥6 shock that has struck since Ch-Chi. Earthquakes are mapped in Figure 2b inset. No preferred plane has been proposed for event 10.

Figure Captions

Figure 1. M≥2 seismicity during (a), the 50 months preceding the 1999 Chi-Chi earthquake and the 50 months afterward, and (b), beginning 3 months after the mainshock.

Figure 2: Focal mechanism distribution for events in and around Taiwan (a) before and (b) after the Chi-Chi mainshock. The focal mechanisms are the available moment tensor solutions from Broadband Array in Taiwan for Seismology (BATS). M_W is about 0.19 less than the local magnitude (M_L) determined in the catalog, and M_c=4.2. The M≥6 shocks are shown in the inset in (b), with the preferred rupture plane indicated by the bold line. Event numbers correspond to Table 2, and the references are: **a**, Chi and Dreger (2004); **b**, Yen (2002); **c**, Ma and Wu (2001).

Figure 3. The minimum magnitude of completeness, Mc, for 50-month pre- and post-Chi Chi periods, calculated from ZMAP. The post-Chi Chi period begins 3 months after the mainshock are omitted. The cell size is increased offshore to capture sufficient earthquakes for M_c determination.

Figure 4. Calculated seismicity rate change associated with the Chi-Chi earthquake. For the 20 x 20 x 30 km cells, M≥2 shocks are used; for the 40 x 40 x 30 km cells, M≥3 are used, based on the distribution of M_c as shown in Figure 3. Contours 0.25-bar Coulomb stress increase (solid) and decrease (dashed) from Figure 7d are superimposed on the seismicity rate change.

Figure 5. (a) M≥3 seismicity during the 50 months before and after the Chi-Chi earthquake. Based on the M≥3 observations and the fixed cell-size calculations of Figure 4, sites of apparent seismicity rate increase are colored light orange; sites of decrease are colored turquoise. Site names correspond to Figure 6.

Figure 6. Time series of the zones of seismicity rate drop identified in Figure 5, each at $M \geq M_c$ so that detection is uniform throughout the period shown. For each zone, M_c was determined independently in ZMAP (Wiemer, 2001). The horizontal lines mark the mean pre and post-Chi Chi seismicity rates, with the 3-month period after Chi-Chi excluded.

Figure 7. Maximum Coulomb failure stress change within the seismogenic crust for idealized Chi-Chi ruptures, for $\mu'=0.4$. The source is 78 km long and dips 29°E. (a-b)

Stress resolved on optimally oriented thrust or strike-slip faults with E-W regional compression and a source rake of 90°. (b-c) Stress resolved on optimally oriented thrust and strike-slip faults with 122° regional compression and a source strike of 3° and rake of 66°.

Figure 8. Slip distribution from Ji et al. (2003), with a main segment 80-km-long north-south segment, a 20-km-long segment to the southwest and a 30-km-long segment to the northeast. Each fault segment has a width of about 34 km and dips 29° to the east. The fault plane in each segment was approximated by the subfaults with equal area of 3.8 km x 3.7 km.

Figure 9. Coulomb stress changes on optimally oriented thrust (a), strike-slip (b) and normal (c) faults at four depth intervals, together will all M≥4 shocks with focal mechanisms. Stress is calculated at the center of each interval. Green shocks occurred during the 50 months before Chi-Chi, magenta shocks struck during the succeeding 50 months. Shallower intervals are not shown because no focal mechanisms are located above 9 km depth.

Figure 10. Stress change on nodal planes for all events with focal mechanisms. (a) Shear stress change on post-Chi Chi nodal planes. (b) Coulomb stress change. For earthquakes with positive ΔCFF values on either nodal plane, the smaller of the two is chosen. For the earthquakes for which only one nodal plane has a positive ΔCFF, the positive one is chosen. For the events with negative ΔCFF on both nodal planes, the smaller absolute value is chosen. (c) Coulomb stress change calculated in the same manner for the pre-Chi

Chi focal mechanisms, which serves as a control sample. (d) The percentage of nodal planes with a calculated Coulomb stress change greater than 0.1 bar for the pre- and post-Chi Chi periods, showing an increase following the Chi-Chi mainshock.

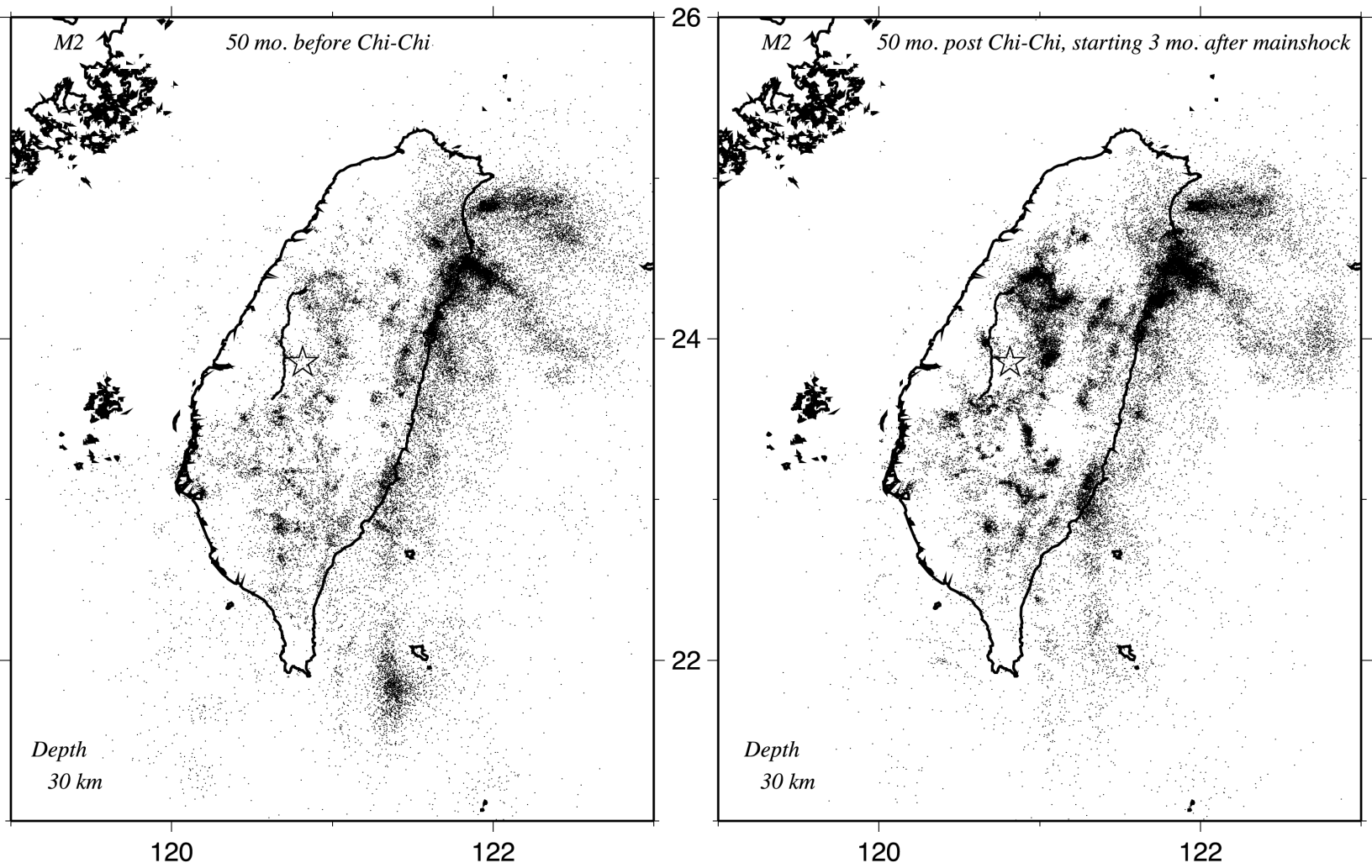
M2
50 mo. before Chi-Chi
Depth
30 km
M2
50 mo. post Chi-Chi, starting 3 mo. after mainshock
Depth
30 km
26
24
22
120
122
120
122

Figure 1

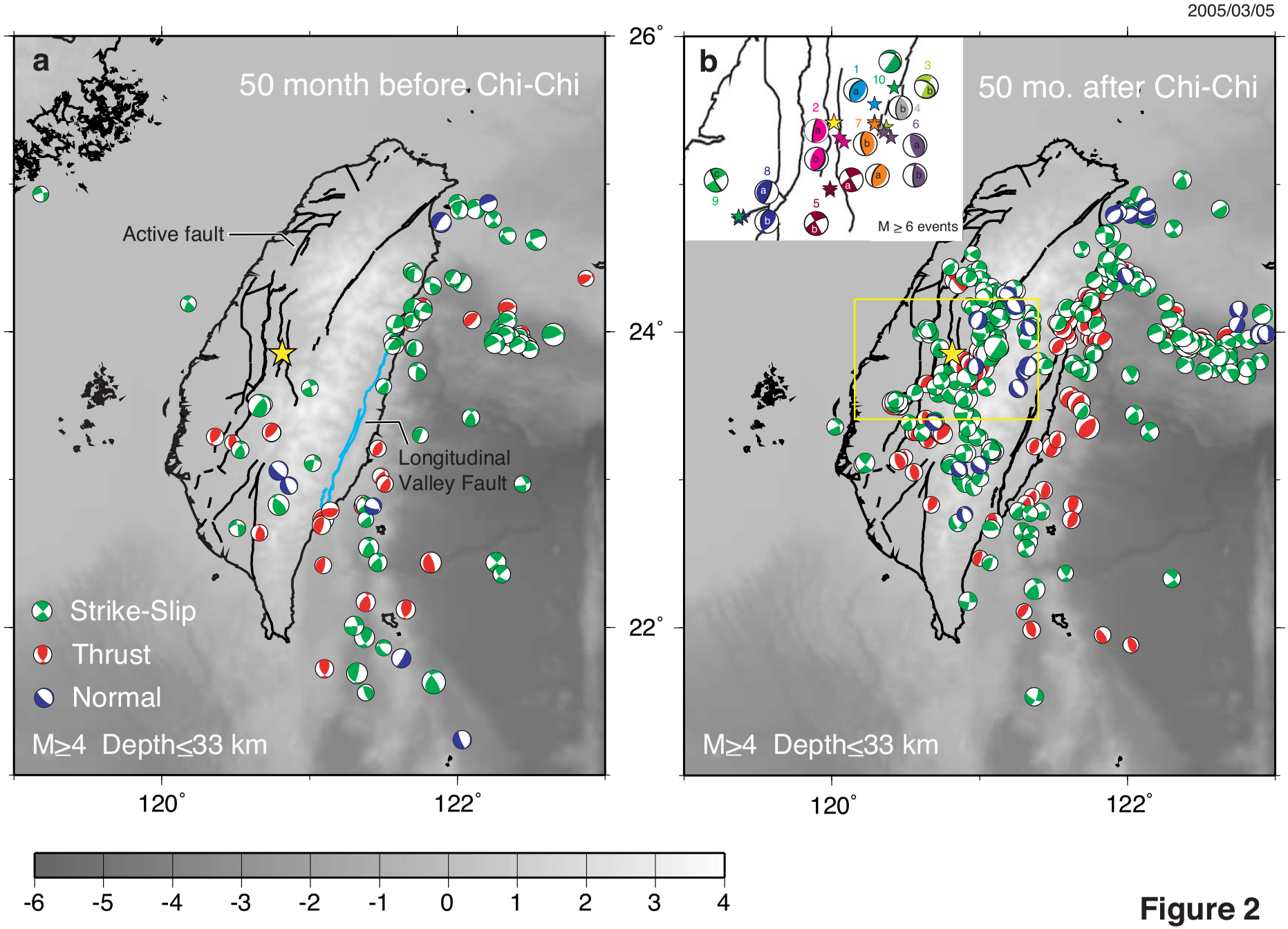
2005/03/05
a
50 month before Chi-Chi
Active fault
Longitudinal
Valley Fault
Strike-Slip
Thrust
Normal
M≥4 Depth≤33 km
b
50 mo. after Chi-Chi
M ≥ 6 events
M≥4 Depth≤33 km
26°
24°
22°
120°
122°
-6 -5 -4 -3 -2 -1 0 1 2 3 4

Figure 2

2005/02/25

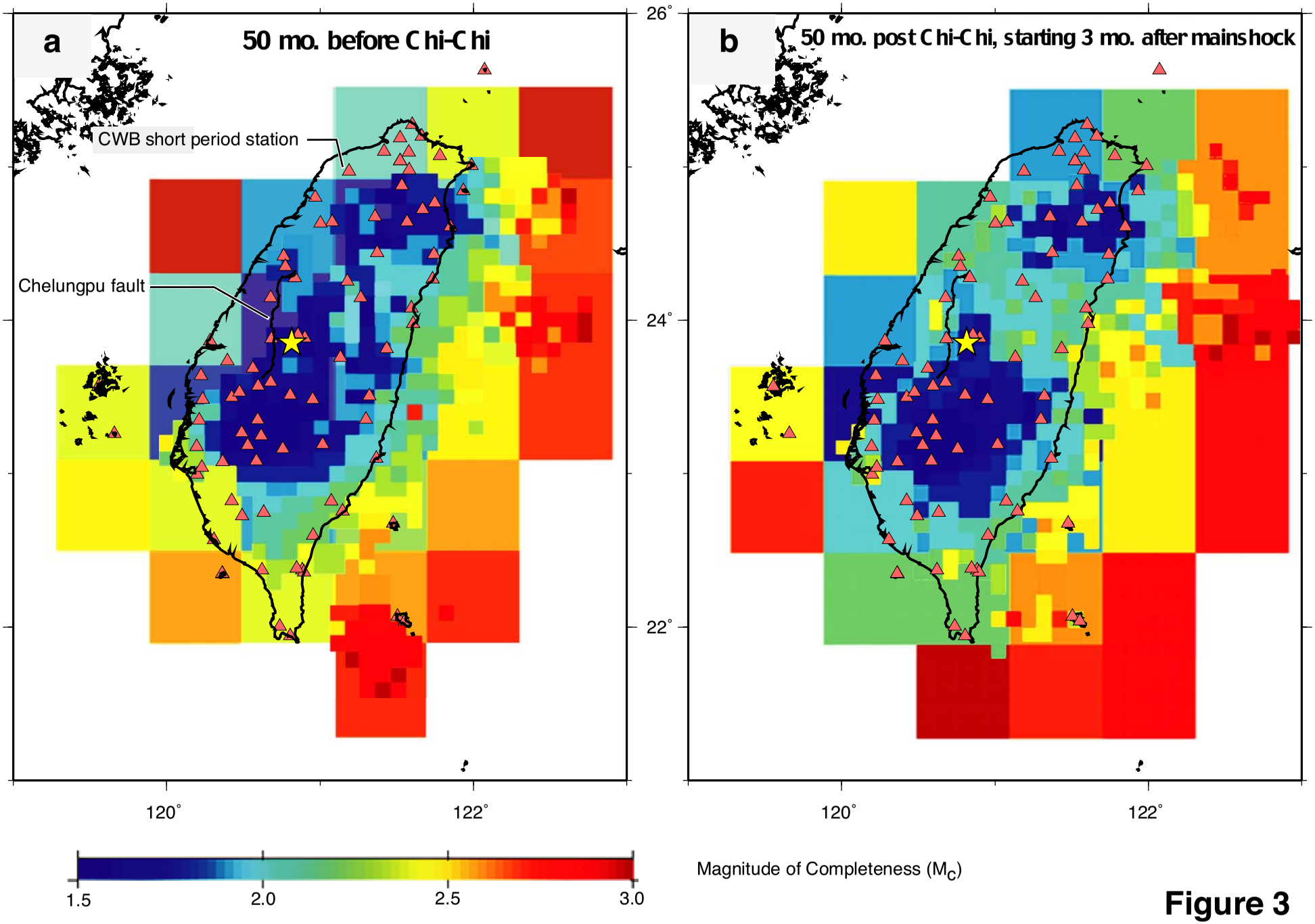

Figure 3

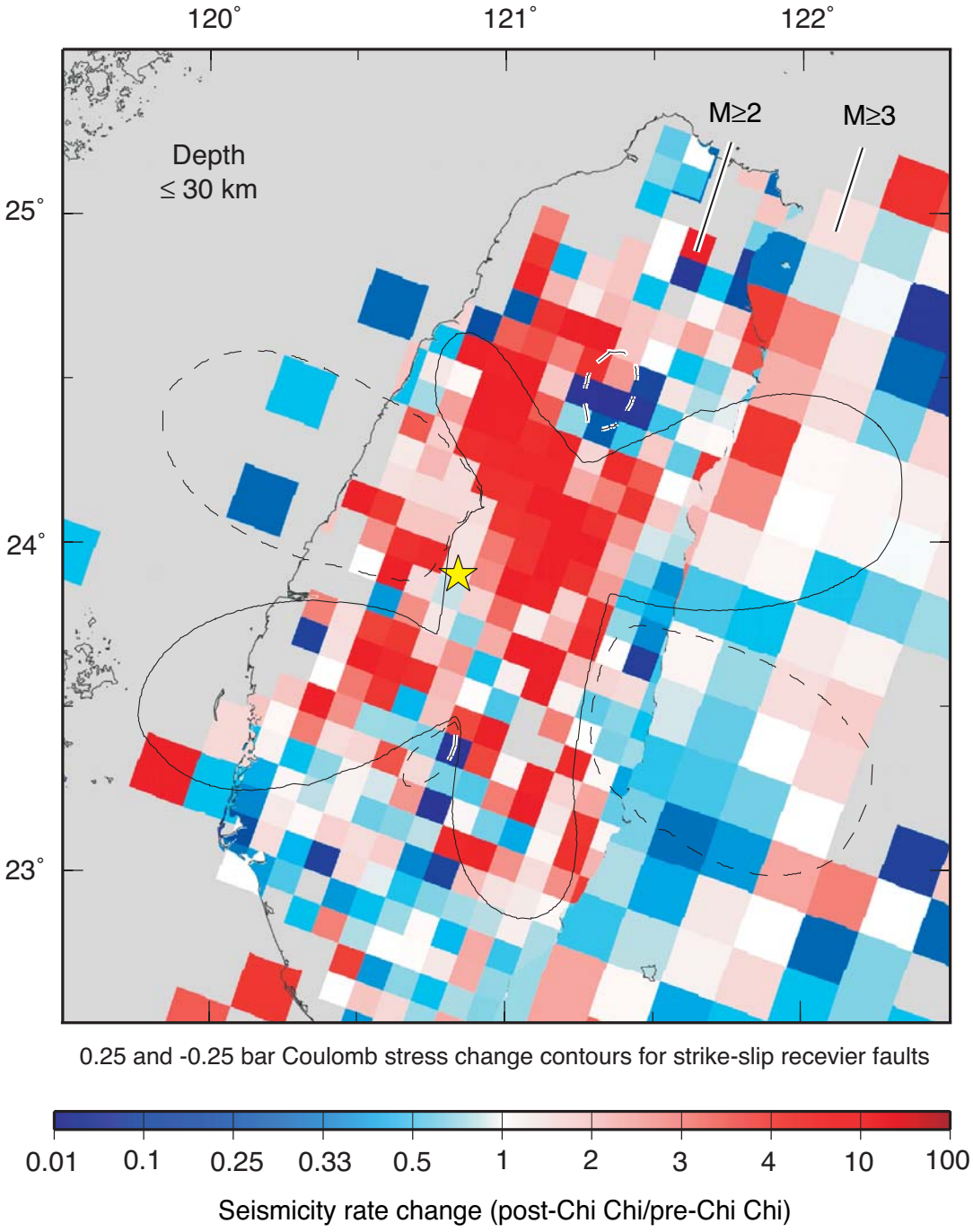
120°
121°
122°
25°
24°
23°
Depth
≤ 30 km
M≥2
M≥3
0.25 and -0.25 bar Coulomb stress change contours for strike-slip recevier faults
0.01
0.1
0.25
0.33
0.5
1
2
3
4
10
100
Seismicity rate change (post-Chi Chi/pre-Chi Chi)

Fig. 4
4 Mar

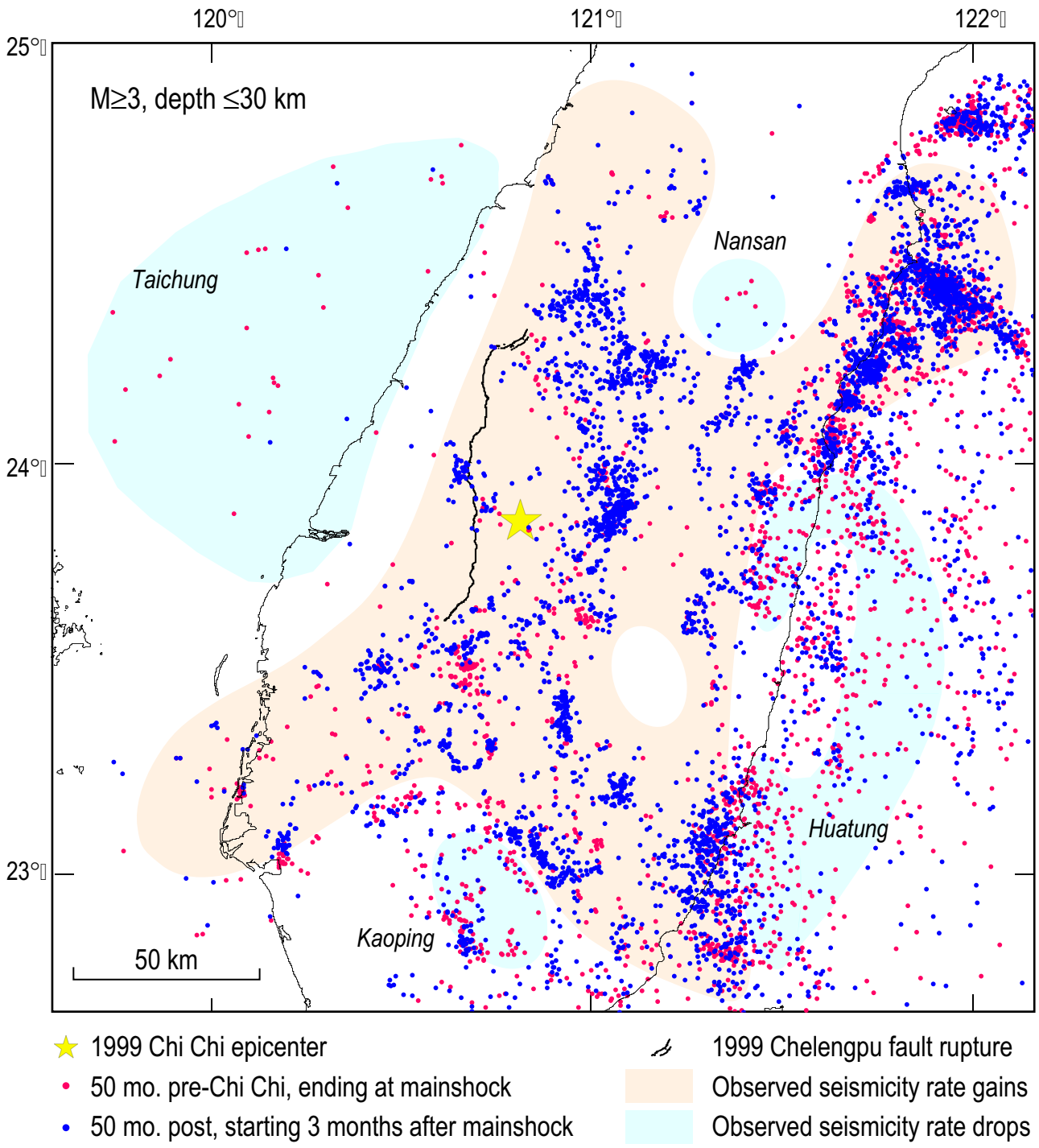
120°
121°
122°
25°
24°
23°
M≥3, depth ≤30 km
Taichung
Nansan
Huatung
Kaoping
50 km
1999 Chi Chi epicenter
50 mo. pre-Chi Chi, ending at mainshock
50 mo. post, starting 3 months after mainshock
1999 Chelengpu fault rupture
Observed seismicity rate gains
Observed seismicity rate drops

Fig 5
3 Mar 05

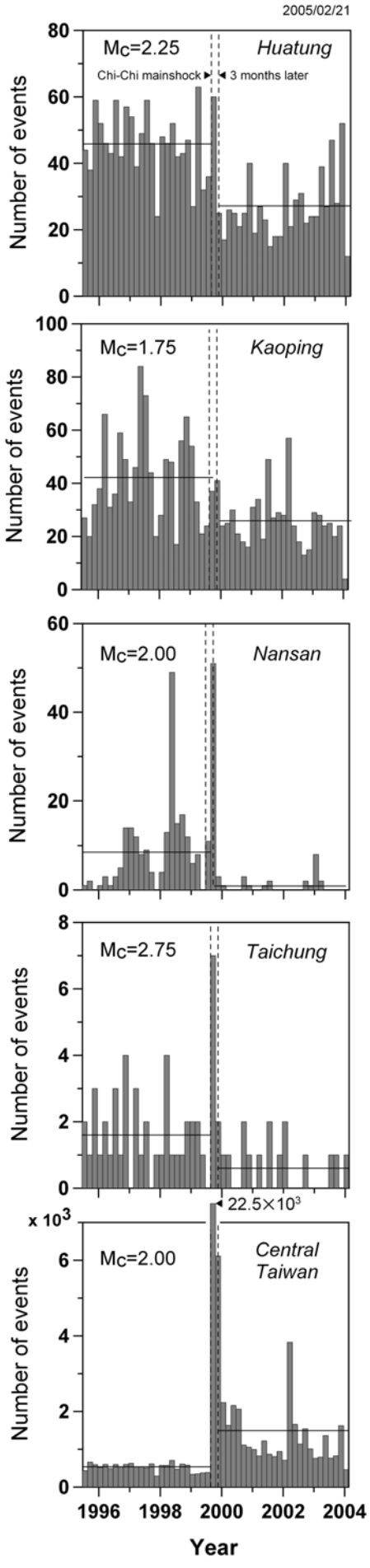
2005/02/21
Mc=2.25
Huatung
Chi-Chi mainshock
3 months later
Number of events
Mc=1.75
Kaoping
Mc=2.00
Nansan
Mc=2.75
Taichung
22.5×10³
x 10³
Mc=2.00
Central Taiwan
1996
1998
2000
2002
2004
Year

Figure 6

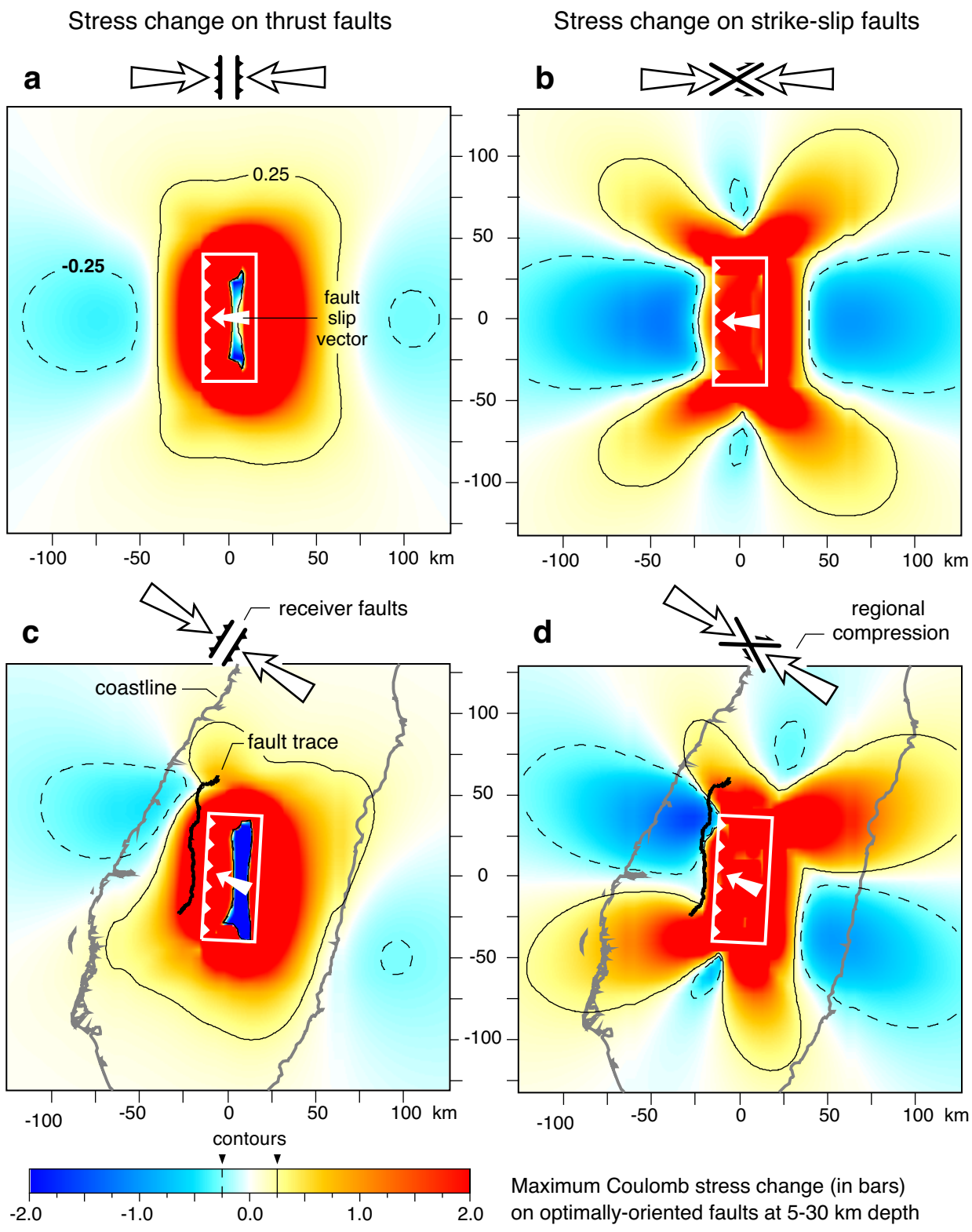
Stress change on thrust faults
Stress change on strike-slip faults
a
b
0.25
-0.25
fault
slip
vector
100
50
0
-50
-100
-100
-50
0
50
100 km
c
d
receiver faults
regional
compression
coastline
fault trace
contours
-2.0
-1.0
0.0
1.0
2.0
Maximum Coulomb stress change (in bars)
on optimally-oriented faults at 5-30 km depth

Fig. 7
3 Mar 05

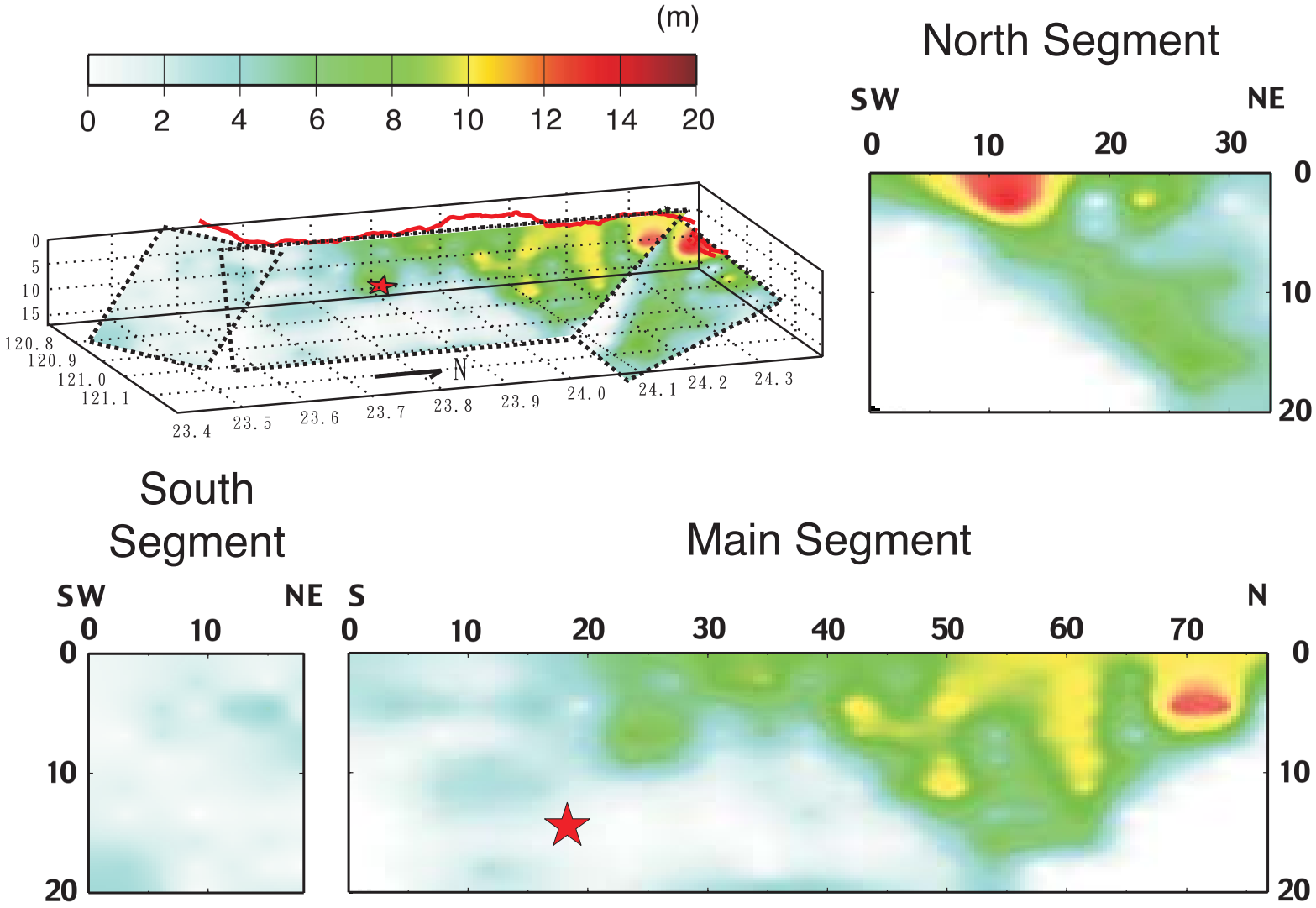
(m)
0 2 4 6 8 10 12 14 20
0
5
10
15
120.8
120.9
121.0
121.1
23.4 23.5 23.6 23.7 23.8 23.9 24.0 24.1 24.2 24.3
N
North Segment
SW
NE
0 10 20 30
0
10
20
South Segment
SW
NE
0 10
0
10
20
Main Segment
S
N
0 10 20 30 40 50 60 70
0
10
20

Figure 8

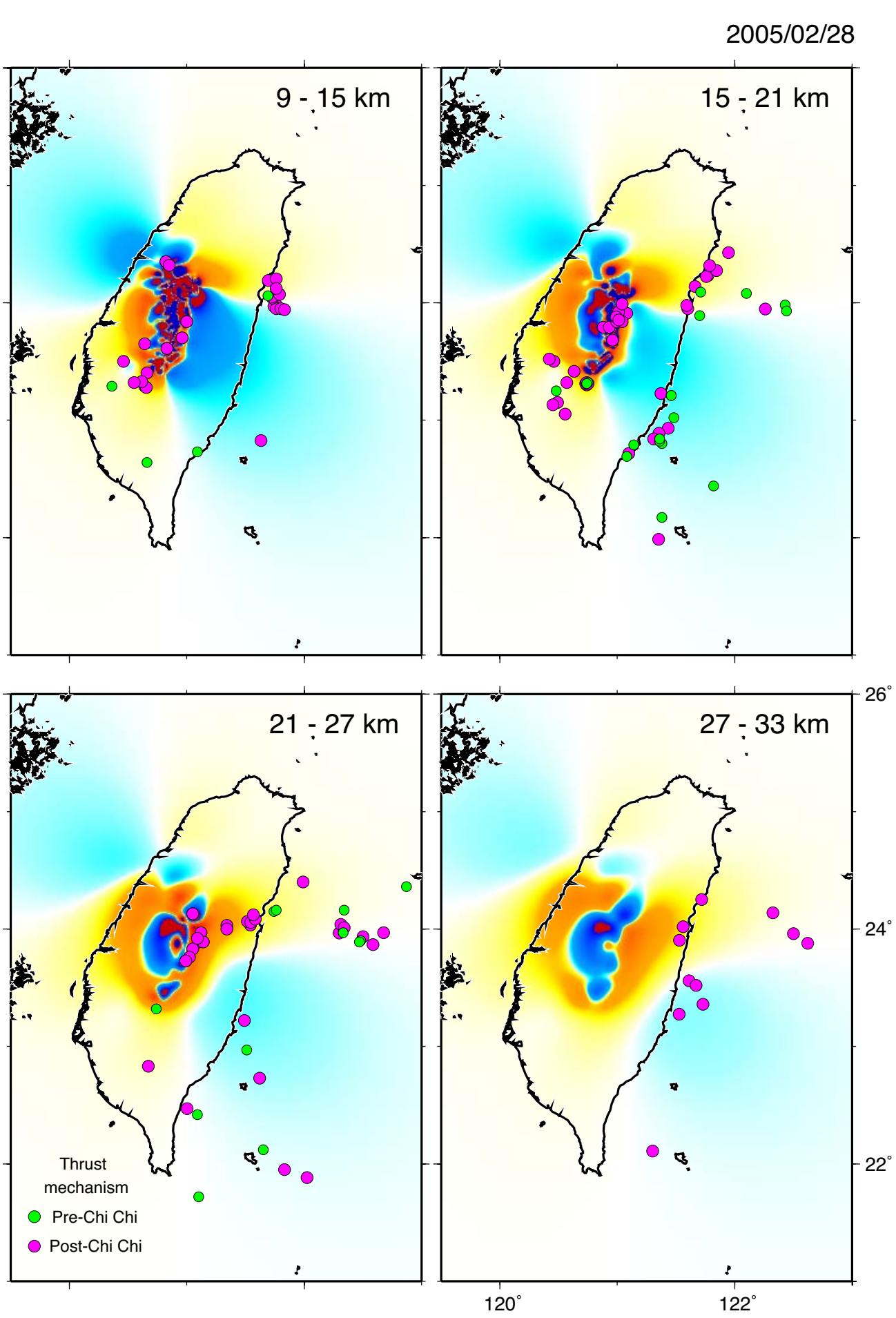
2005/02/28
9 - 15 km
15 - 21 km
21 - 27 km
27 - 33 km
26˚
24˚
22˚
120˚
122˚
Thrust
mechanism
Pre-Chi Chi
Post-Chi Chi
-10.0 -1.0 -0.5 -0.3 -0.1 0.0 0.1 0.3 0.5 1.0 10.0
Coulomb stress change on thrust faults (bars)

Figure 9a

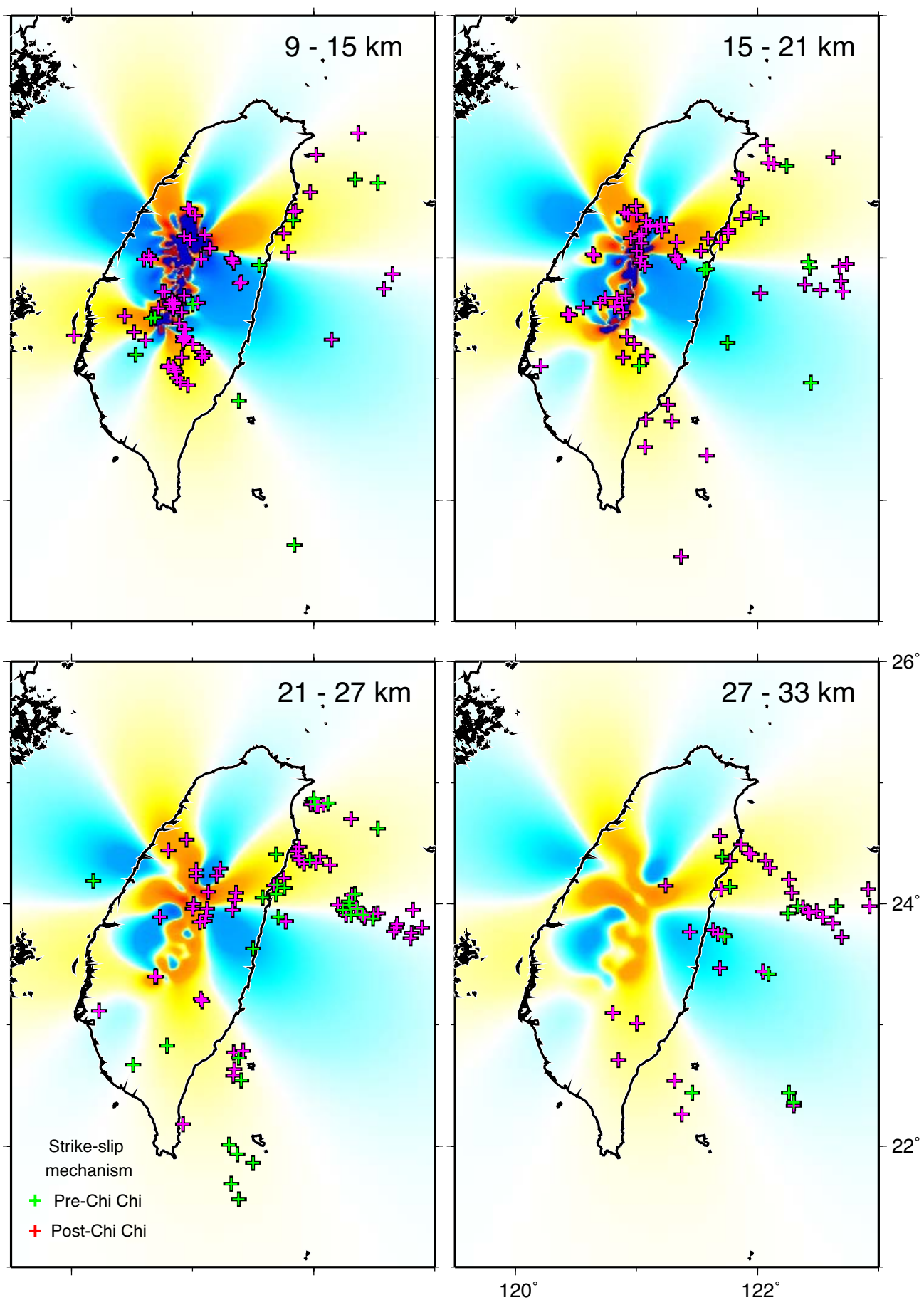
2005/02/28
9 - 15 km
15 - 21 km
21 - 27 km
27 - 33 km
26˚
24˚
22˚
120˚
122˚
Strike-slip
mechanism
Pre-Chi Chi
Post-Chi Chi
-10.0 -1.0 -0.5 -0.3 -0.1 0.0 0.1 0.3 0.5 1.0 10.0
Coulomb stress change on strike-slip faults (bars)

Figure 9b

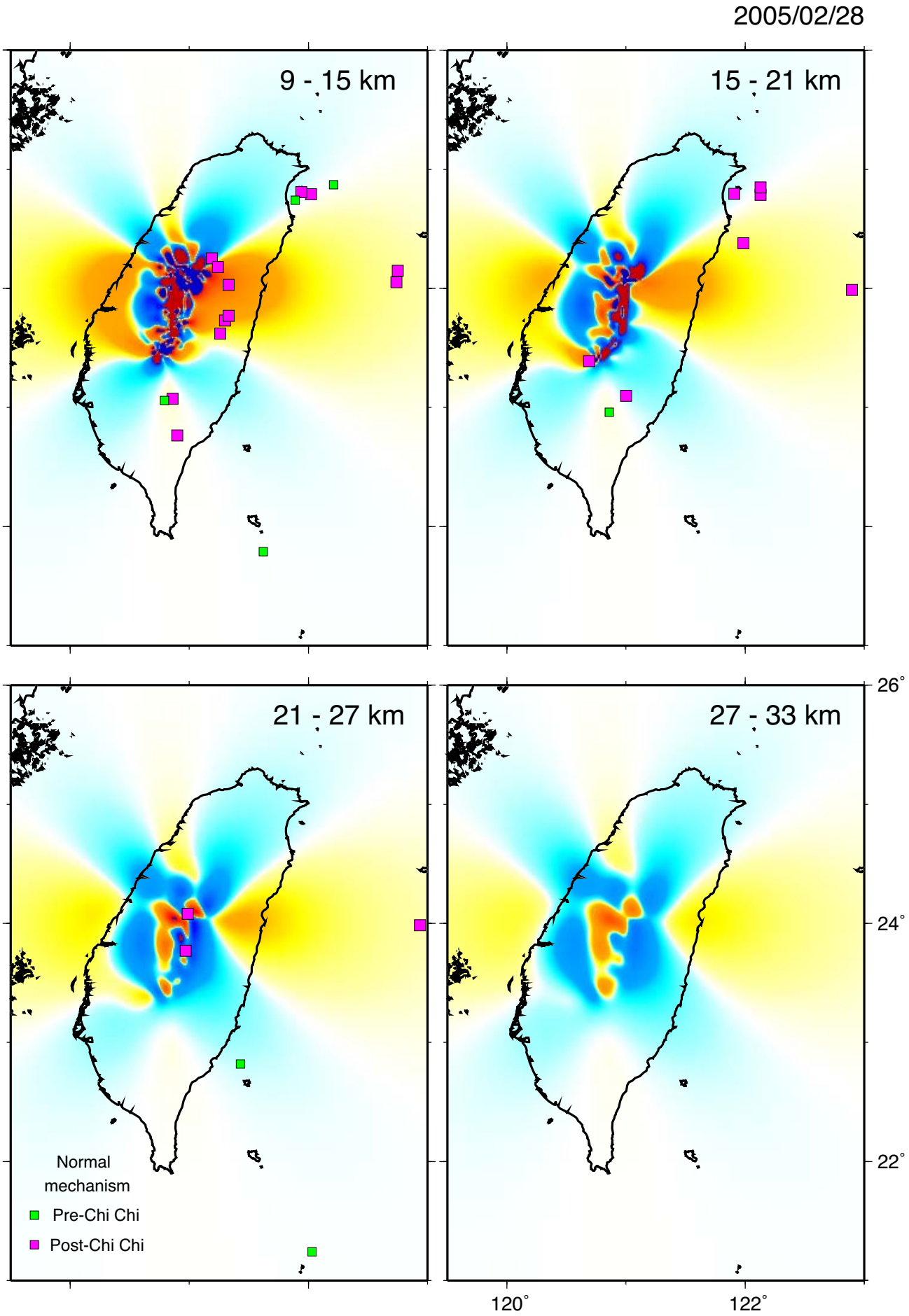
2005/02/28
9 - 15 km
15 - 21 km
21 - 27 km
27 - 33 km
26˚
24˚
22˚
120˚
122˚
Normal mechanism
Pre-Chi Chi
Post-Chi Chi
-10.0 -1.0 -0.5 -0.3 -0.1 0.0 0.1 0.3 0.5 1.0 10.0
Coulomb stress change on normal faults (bars)

Figure 9c

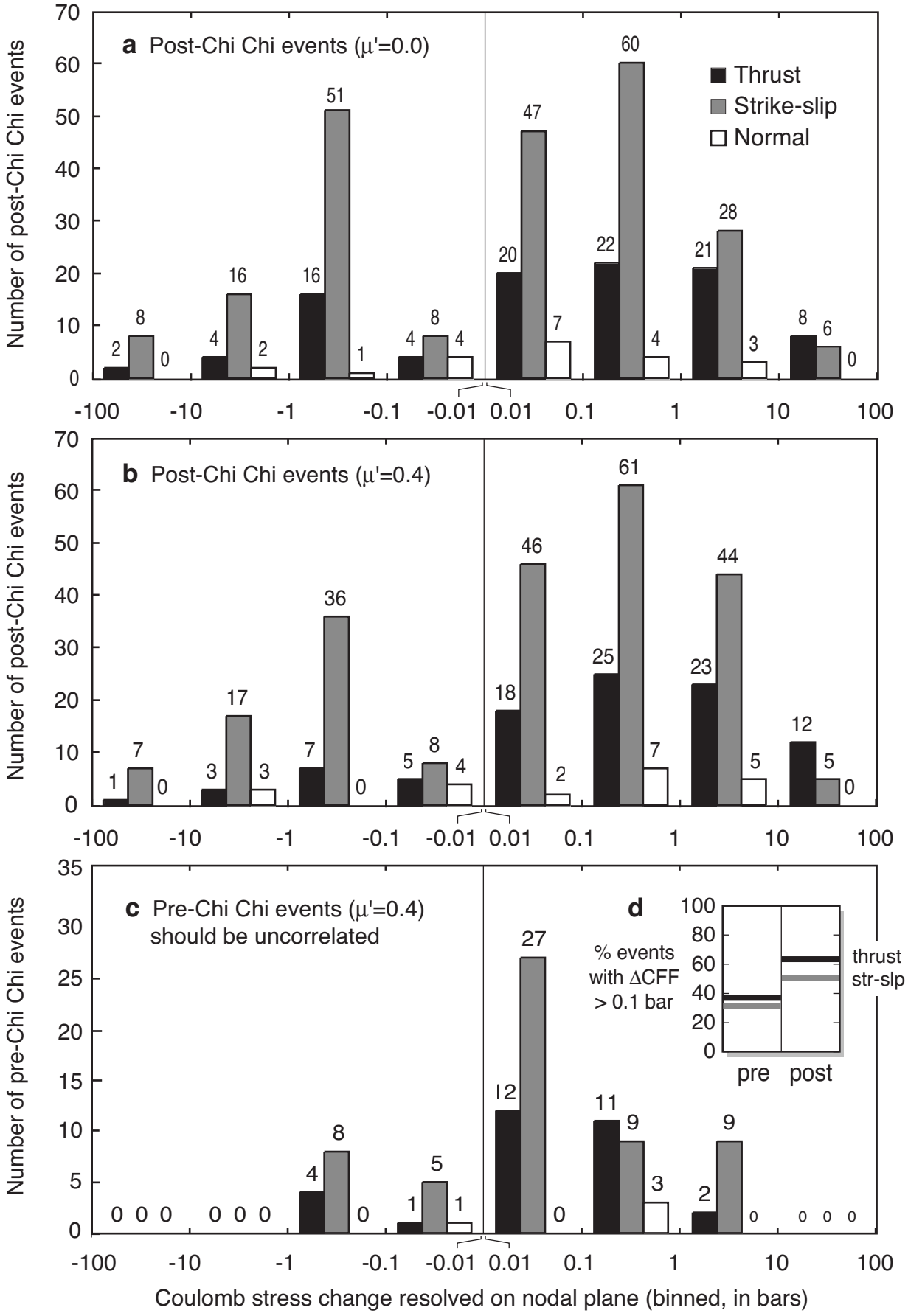

Fig. 10
5 Mar 05

	Azimuth (°)	Inclination (°)	Magnitude (bars)
σ1	122	0	100
σ2	32	0	30
σ3	122	90	0

Table 1

Event	Date	Time	Reference	Mag. Mw	Depth (km)	Lon. (°)	Lat. (°)	Strike (°)	Dip (°)	Rake (°)	Chi-Chi ΔCFF (bar)	Cumulative ΔCFF (bar)
1	1999/9/20	17:57:15	Chi and Dreger (2004)	6.4	8	121.01	23.94	200	41	78	-1.9	-1.9
2	1999/9/20	18:03:41	Chi and Dreger (2004)	6.2	8	120.86	23.81	0	10	80	57.9	57.9
			Yen (2002)	6.2	18	120.88	23.79	23	33	95	3.1	3.2
3	1999/9/20	18:11:53	Yen (2002)	6.1	24	121.06	23.85	209	85	139	7.3	-5.7
4	1999/9/20	18:16:16	Yen (2002)	6.1	21	121.04	23.84	336	38	63	14.8	14.6
5	1999/9/20	21:46:38	Chi and Dreger (2004)	6.6	18	120.82	23.60	330	89	15	2.6	2.5
			Yen (2002)	6.3	12	120.82	23.60	75	67	186	7.8	7.8
6	1999/9/22	00:14:41	Chi and Dreger (2004)	6.2	10	121.08	23.81	165	70	100	6.9	7.1
			Yen (2002)	6.2	29	121.05	23.83	314	26	43	3.0	2.9
7	1999/9/25	23:52:49	Chi and Dreger (2004)	6.8	16	121.01	23.87	5	30	100	11.5	11.3
			Yen (2002)	6.4	15	121.01	23.86	32	32	102	13.2	11.9
8	1999/10/22	02:18:56	Chi and Dreger (2004)	6.4	16	120.45	23.53	20	75	90	0.3	0.3
			Ma and Wu (2001)	6.4	17	120.43	23.52	180	42	56	0.0	0.0
9	1999/10/22	03:10:17	Ma and Wu (2001)	6.0	17	120.43	23.53	60	90	170	0.3	-1.7
10	2000/6/10	18:23:00	DMC-IES	6.1	27	121.11	23.9	296	24	-8	5.7	6.0
								33	87	-114	2.2	2.3
									Median		4.4	3.0
									Average		8.4	7.4

Table 2